On cracked rotating shaft mechanics: a systematic approach

Saber El Arem[1], Maha Ben Zid[2]

[1] *LAMPA, Arts et Métiers ParisTech, saber.elarem@ensam.eu*
[2] *R&T, IUT Saint Malo, maha.benzid@univ-rennes1.fr*

Résumé — We present a systematic approach to deal with the modeling and analysis of the cracked rotating shafts behaviour. We begin by revisiting the problem of modelling the breathing mechanism of the crack. Here we consider an original approach based on the form we give to the energy of the system and then identify the mechanism parameters using 3D computations with unilateral contact conditions on the crack lips. A dimensionless flexibility is identified which makes the application of the approach to similar problems straightforward. The additional flexibility due to the crack is then introduced in a simple and comprehensive dynamical system (2 DOF) to characterize the crack effects on the dynamical response of a rotating shaft. Many results could help in early crack detection.
Mots clés — cracked shafts breathing crack rotordynamics instability

1 Introduction

In dealing with cracked shafts mechanics, we mainly distinguich two aspects :

1. The first one is to model the effects of the crack presence on the static behaviour of the shaft. When the shaft rotates, the crack opens and closes (breathes) and the resulting additional flexibility should be identified for all angular positions. The modeling and identification of this breathing mechanism are crucial since it measurably affects the dynamics of the system.
2. The second is the examination of the vibrational response of the system to clearly identify the effects of the crack presence and suggest parameters that could help in developping an efficient methodology for early crack detection.

The approach presented in this article inherits from the EDF−LMS modeling procedures. We concentrate the additional flexibility related to the crack in one single parameter (function) that depends on the system response (nonlinear). But, in this work, we identify a cracked beam element which is different from the nodal representation adopted in [1]. Second, we present a dimensionless flexibility due to the crack wich is dependent only on the crack properties (geometry, relative depth) that can be used straightforward and without any additional 3D computations in similar problems. And, to make this approach generic and easy to adopt by engineers and scientists, we give an explicit polynomial function that approximates the additional flexibility due to the cracked transverse section. Thus, the procedure of identification could be skipped by those who will have adopted the approach described here, and this represents an important saving of time for scientists and powerplant operators. Our main objective in this article is to present a methodological approach in dealing with cracked shafts.

2 Breathing mechanism modeling and identification

The three-dimensional FE model considered is that of a cylinder of axis (oz), radius R, length L, containing, at midspan, a cracked transverse section, cf. Figure 1. The structural element, clamped at its both ends ($z = 0$ and $z = L$), is subjected at $z = \dfrac{L}{2}$ to a force $\mathbf{F} = (F_\xi, F_\eta)$.

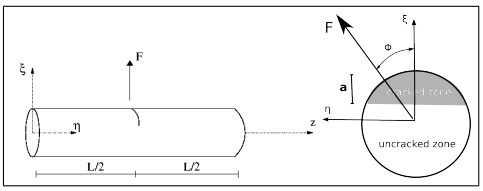

FIGURE 1 – The current 3D model

Let W^* be the total elastic (complementary) energy of the system. According to [1] and [2], W^* can be put in the form :

$$W^*(\mathbf{F}) = W_s^*(\mathbf{F}) + w_c^*(\mathbf{F}) \tag{1}$$

where W_s^* denotes the total elastic energy of the uncracked structure under the loading $\mathbf{F}$, and $w_c^*(\mathbf{F})$ the additional elastic energy due to the presence of the crack. Some properties of the problem energy will make easier the identification of the flexibility due to the crack presence ([1], [2]).

Property 1 :

w_c^* is **strictly convex and positively homogeneous of degree 2** :

$$\forall \lambda \geq 0 \, , \, w_c^*(\lambda \mathbf{F}) = \lambda^2 w_c^*(\mathbf{F}) \tag{2}$$

Property 1 comes from the fact that the contact surface between the crack lips (and therefore the additional flexibility) does not depend on $||F||$ but only on the direction of $\mathbf{F}$. It should be noticed that an essential hypothesis for obtaining *propertie* 1 is that the gap between the lips of the crack is zero in the unstressed configuration which distinguishes the crack from a notch.
A raisonable choice for w_c^* is to consider a quadratic form of $\mathbf{F}$. We write :

$$w_c^*(\mathbf{F}) = \frac{1}{2} s_c(\mathbf{F}) ||\mathbf{F}||^2 \tag{3}$$

$s_c(\mathbf{F})$ represents the additional flexibility of the structure due to the crack presence to be identified by means of 3D computations.

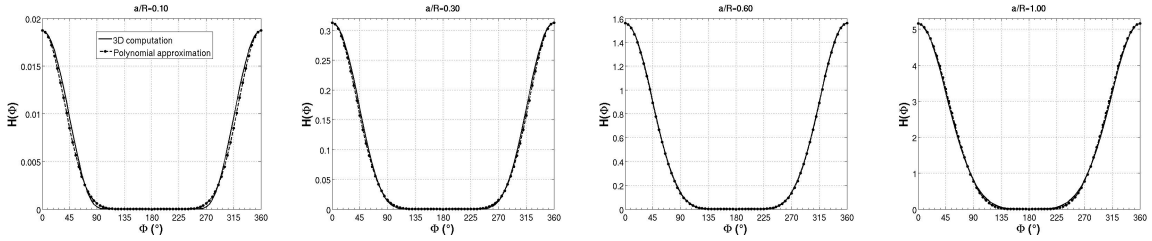

FIGURE 2 – Dimensionless flexibility as a function of loading angle for different crack depth

With *Property* 1, the problem of identification of the function w_c^* on $\mathbb{R}^2$ is reduced to the identification of the flexibility function $s_c(\Phi)$ on the interval $[0, 2\pi]$ by considering :

$$\mathbf{F} = (F_\xi, F_\eta) = (\cos(\Phi), \sin(\Phi)) \ , ||F|| = 1 \text{ and } \Phi = atan(\frac{F_\eta}{F_\xi})$$

The total elastic energy of the system could be written :

$$W^*(\mathbf{F}) = \frac{1}{2} s(\Phi) ||\mathbf{F}||^2 = \frac{1}{2} \{s_0 + s_c(\Phi)\} ||\mathbf{F}||^2 \tag{4}$$

where s_0 is a constant representing the bending flexibility of the uncracked shaft. Instead of identifying the function $s_c(\Phi)$, it would be more advantageous to identify a parameter that lets appear the intrinsic properties of the crack. Thus, a dimensionless coefficient that only depends on the crack parameters (geometry, depth, etc...) would be more useful to identify. This aims to make our approach generic and easily exploitable in similar configurations. we write :

$$W^*(\mathbf{F}) = \frac{1}{2} s(\Phi) ||\mathbf{F}||^2 = \frac{1}{2} \left\{ s_0 + \frac{L^2}{48\pi E R^3} H(\Phi) \right\} ||\mathbf{F}||^2 \tag{5}$$

Given a crack geometry and a loading direction Φ , the dimensionless flexibility H represents a measure of the open (closed) parts of the crack. E is the Young's modulus of the material.

2.1 Identification procedure of the dimensionless flexibility H :

Three-dimensional computations have been carried out to determine H for the case presented in Figure 1. The structure contains a crack with a rectilinear tip at midspan. The clamped shaft element is subjected to $\mathbf{F}$ and the angle Φ is varied in [0°,360°] at a rate of a loading case every 5° and, thus, a total of 72 loading cases where carried out. The identification of H also requires the realization of similar computations on the uncracked structure. Knowing the forces ($\mathbf{F}$) and the displacements ($\mathbf{u}$) at the cracked section, the formula of Clapeyron makes it easy to evaluate W_s^* and W^* of the uncracked and the cracked structures, respectively ([3], [4]). w_c^* is obtained by :

$$w_c^*(\Phi) = W^*(\Phi) - W_s^*(\Phi) \ , \forall \Phi \in [0,360] \tag{6}$$

then H is computed using :

$$H(\Phi) = w_c^*(\Phi)\frac{48\pi E R^3}{L^2} \ , \forall \Phi \in [0,360] \tag{7}$$

Figure 2 shows that for cracks with a rectilinear tip and a relative depth $\frac{a}{R} < 1.0$, the crack is fully open when $\Phi = 0°$ (or 360°) and closes completely on an interval arround $\Phi = 180°$. In fact, despite the rotation, shallow cracks may remain totally into the compressed half-section before going into the taut zone. This interval reduces to $\Phi = 180°$ when $\frac{a}{R} = 1$. Between these loading cases, the crack is partially open. The evolution from totally open to totally closed crack is smooth and regular.

When $\frac{a}{R} > 1.0$, the crack can not be fully closed since it can not be completely contained in the compressed half-section for any $\Phi \in [0,360°]$. In this case, $H(\Phi) > 0$ and its lowest value is reached at $\Phi = 180°$.

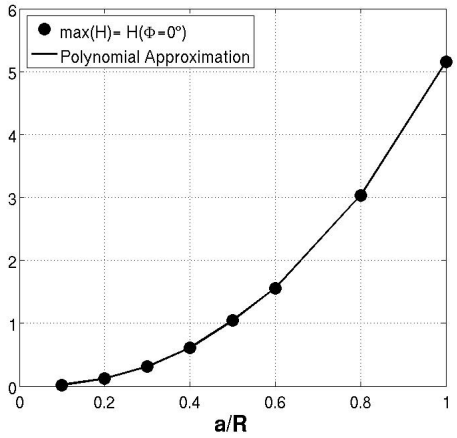

FIGURE 3 – Maximum of dimensionless flexibility as a function of crack depth

In Figure 3 we present the maximum of additional flexibility ($max(H)$) as a function of the relative depth of the crack ($\frac{a}{R}$). By adopting a polynomial fitting we wrote :

$$\max(H)(\frac{a}{R}) = P_a(\frac{a}{R}) = \sum_{i=0}^{7} c_i(\frac{a}{R})^i \tag{8}$$

Also, we have found that a good fitting of the values of H would be :

$$\begin{aligned} H(\Phi) &= max(H)\left\|\sin(\frac{\Phi+\pi}{2})\right\|^{Q_a(\frac{a}{R})} \\ &= P_a(\frac{a}{R})\left\|\sin(\frac{\Phi+\pi}{2})\right\|^{Q_a(\frac{a}{R})} \end{aligned} \tag{9}$$

with Q a polynomial function of $\frac{a}{R}$ given by :

$$Q_a(\frac{a}{R}) = \sum_{i=0}^{7} q_i(\frac{a}{R})^i \tag{10}$$

In Figure 2 we can see that the polynomial approximation of H using (9) produces an excellent fitting for cracks with rectilinear tip and width $\frac{a}{R} \leq 1.0$. We can easily extend the approach for deeper cracks by considering a formula similar to (9) and adding a constant term (which is $min(H) = H(\Phi = \pi)$) that increases with the crack depth. In this first article devoted to this new systematic approach, we want to focus on shallower cracks since we aim to characterize cracks effects before they become of critical depth.

2.2 Constitutive equations

As mentioned earlier, our objective is to build a beam model based on realistic 3D model to be extensively used in the nonlinear dynamics of cracked rotating shafts. The nonlinear constitutive equations

at the cracked section (midspan) are obtained by differentiating W^* with respect to $\mathbf{F}$. we write :

$$\mathbf{u} = \begin{pmatrix} u_\xi \\ \\ u_\eta \end{pmatrix} = \mathbf{S}(\Phi) \begin{pmatrix} F_\xi \\ \\ F_\eta \end{pmatrix} = \{\mathbf{S_0} + \mathbf{S_c}(\Phi)\} \begin{pmatrix} F_\xi \\ \\ F_\eta \end{pmatrix} = \begin{pmatrix} s_0 + s_c(\Phi) & -\frac{1}{2}s'_c(\Phi) \\ \\ \frac{1}{2}s'_c(\Phi) & s_0 + s_c(\Phi) \end{pmatrix} \begin{pmatrix} F_\xi \\ \\ F_\eta \end{pmatrix} \tag{11}$$

where $\mathbf{S_0}$ and $\mathbf{S}$ are, respectively, the flexibility matrices of the uncracked and cracked shaft.

$$s'_c(\Phi) = \frac{ds_c(\Phi)}{d\Phi} = \frac{L^2}{48\pi ER^3}\frac{dH(\Phi)}{d\Phi} = \frac{L^2}{48\pi ER^3}H'(\Phi) \tag{12}$$

Finally, at the cracked section we have :

$$\begin{pmatrix} u_\xi \\ \\ u_\eta \end{pmatrix} = \left\{ \begin{pmatrix} s_0 & 0 \\ \\ 0 & s_0 \end{pmatrix} + \frac{L^2}{48\pi ER^3} \begin{pmatrix} H(\Phi) & -\frac{1}{2}H'(\Phi) \\ \\ \frac{1}{2}H'(\Phi) & H(\Phi) \end{pmatrix} \right\} \begin{pmatrix} F_\xi \\ \\ F_\eta \end{pmatrix} \tag{13}$$

The extradiagonal terms show that the crack introduces coupling between the transverse directions of the shaft element. In numerical codes for structural analysis, we usually prefer a relation of the form :

$$\begin{pmatrix} F_\xi \\ \\ F_\eta \end{pmatrix} = \{\mathbf{S}(\Phi)\}^{-1} \begin{pmatrix} u_\xi \\ \\ u_\eta \end{pmatrix} = \mathbf{K}(\mathbf{u}) \begin{pmatrix} u_\xi \\ \\ u_\eta \end{pmatrix} = \{\mathbf{K_0} - \mathbf{K_c}(\mathbf{u})\} \begin{pmatrix} u_\xi \\ \\ u_\eta \end{pmatrix} \tag{14}$$

where $\mathbf{K_0}$ and $\mathbf{K}$ are, respectively, the stiffness matrices of the uncracked and cracked shaft, with

$$\mathbf{K_0} = \begin{pmatrix} k_0 & 0 \\ 0 & k_0 \end{pmatrix} \text{ and } k_0 = \frac{1}{s_0} \tag{15}$$

$\mathbf{K_c}(\mathbf{u})$ represents the stiffness loss due to the crack and depending on the problem unknowns $\mathbf{u}$ which makes the problem nonlinear. Actually, for a given loading direction Φ, the problem is linear with different stiffness for each angle Φ : The loading angle Φ is equal to the response angle ψ defined by :

$$\psi = atan(\frac{u_\eta}{u_\xi})$$

By writting $\mathbf{K_c}(\mathbf{u})$ in the form :

$$\mathbf{K_c} = \frac{48\pi ER^3}{L^2} \begin{pmatrix} k_{\xi\xi}(\psi) & k_{\xi\eta}(\psi) \\ \\ k_{\eta\xi}(\psi) & k_{\eta\eta}(\psi) \end{pmatrix} \tag{16}$$

we obtain :

$$k_{\xi\xi}(\psi) = k_{\eta\eta}(\psi) = \frac{R}{L} - \frac{4R(L + RH(\Phi))}{(4R^2H(\Phi)^2 + 8LRH(\Phi) + R^2H'(\Phi)^2 + 4L^2)} \tag{17}$$

$$k_{\xi\eta}(\psi) = -k_{\eta\xi}(\psi) = -\frac{2R^2H'(\Phi)}{(4R^2H(\Phi)^2 + 8LRH(\Phi) + R^2H'(\Phi)^2 + 4L^2)} \tag{18}$$

We can notice that

$$k_{\xi\eta}(\psi) = -\frac{1}{2}\frac{dk_{\xi\xi}}{d\psi} = -\frac{1}{2}k'_{\xi\xi}$$

Also, when $H(\Phi) = H'(\Phi) = 0$ (no crack), we have :

$$k_{\xi\xi}(\psi) = k_{\xi\eta}(\psi) = 0$$

Like $\mathbf{S_c}$, $\mathbf{K_c}$ is a skew$-$symmetric matrix. Also, we can easily notice that the stiffness matrix of cracked transverse section is completely identified by one single function $k_{\xi\xi}$ and its derivative.

Finaly, at the cracked transverse section, we have the relation :

$$\begin{pmatrix} F_\xi \\ F_\eta \end{pmatrix} = \left\{ \begin{pmatrix} k_0 & 0 \\ 0 & k_0 \end{pmatrix} - \frac{48\pi ER^3}{L^2} \begin{pmatrix} k_{\xi\xi}(\psi) & -\frac{1}{2}k'_{\xi\xi}(\psi) \\ \frac{1}{2}k'_{\xi\xi}(\psi) & k_{\xi\xi}(\psi) \end{pmatrix} \right\} \begin{pmatrix} u_\xi \\ u_\eta \end{pmatrix} \tag{19}$$

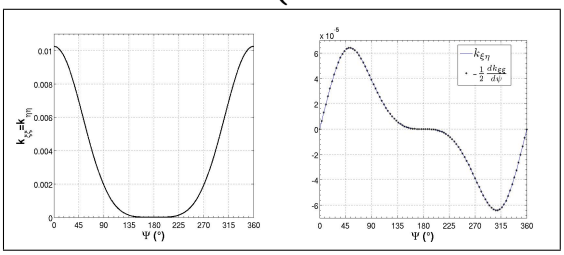

FIGURE 4 – Stiffness loss for $\frac{a}{R} = 1$

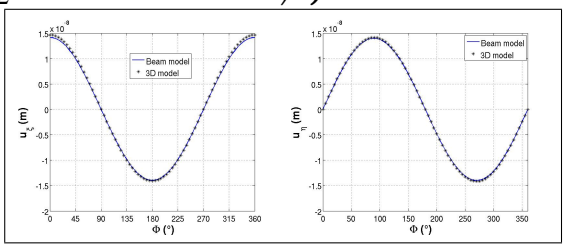

FIGURE 5 – Validation of the procedure for $\frac{a}{R} = 1$

with $k_0 = \frac{192EI}{L^3} = \frac{48\pi ER^4}{L^3}$ the bending stiffness of a biclamped uniform beam. $I = \frac{\pi R^4}{4}$ is the quadratic moment of inertia.

Figure 5 shows an exellent agreement between the 3D results and the beam model. Although the 3D computations consume less than 10 minutes of CPU time, having a reliable and robust beam model is always preferable especially for the examination of the nonlinear dynamics of the system as will be discussed in the next section.

3 Nonlinear dynamics of a rotating shaft with a breathing crack

This section is devoted to the examination of the vibrational response of a De Laval rotor (Figure 6) with the breathing mechanism identified in the first part of this article. To build a systematic approach, we need to remove all the non essential assumptions. We want our methodology to be applicable in the most general configurations. In fact, the new generation of turbines are light weight and often operated at very high frequencies (many times the first critical speed) resulting in hight levels of vibrations. Also in vertical axis machines, the machine self-weight is not the dominant loading. In such configurations, hypothesis of weight dominant situation could not be accepted and we need a robust model capable of handling all possible situations like transient conditions of starting up, coasting down or passing throught resonnance rotating frequencies. In these situations, the vibration levels effects could be the same order of magnitude than the self-weight deflection.

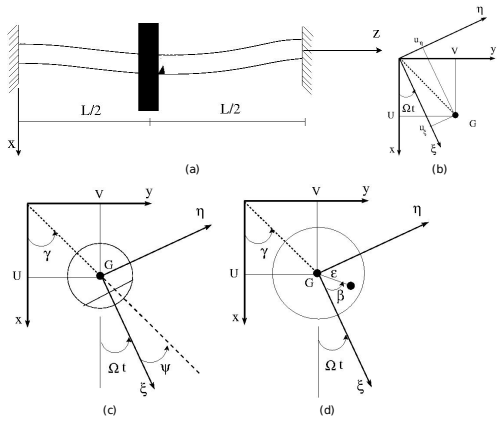

FIGURE 6 – Dynamical system parameters

In the most general case, when considering the modeling of breathing mechanism of the crack in a rotating shaft, we need at each time instant to be able of answering two questions :

1. First, which part of the transverse section is under tension ?
2. Second, where is the cracked part of the transverse section with respect to that taut zone ?

To answer the first question, we need to know the position of the transverse section center G. The position of the crack is given by the rotation angle Ωt. Knowing (U,V) of G and Ωt, we can define in a unique way the stiffness of the structure (Figure 6).

In fact,

$$\psi = atan(\frac{u_\eta}{u_\xi}) = \gamma - \Omega t = atan(\frac{V}{U}) - \Omega t \tag{20}$$

In the rotating, shaft fixed frame $O\xi\eta$, we have established the relation :

$$\begin{pmatrix} F_\xi \\ \\ F_\eta \end{pmatrix} = \left\{ \begin{pmatrix} k_0 & 0 \\ 0 & k_0 \end{pmatrix} - \frac{48\pi ER^3}{L^2} \begin{pmatrix} k_{\xi\xi}(\psi) & -\frac{1}{2}k'_{\xi\xi}(\psi) \\ \\ \frac{1}{2}k'_{\xi\xi}(\psi) & k_{\xi\xi}(\psi) \end{pmatrix} \right\} \begin{pmatrix} u_\xi \\ \\ u_\eta \end{pmatrix} \tag{21}$$

To shift to the inertial frame Oxy, we write :

$$\mathbf{u} = \begin{pmatrix} u_\xi \\ \\ u_\eta \end{pmatrix} = \begin{pmatrix} cos\Omega t & sin\Omega t \\ \\ -sin\Omega t & cos\Omega t \end{pmatrix} \begin{pmatrix} U \\ \\ V \end{pmatrix} = (T(\Omega t))\mathbf{U} \tag{22}$$

Analogously for the forces, we write :

$$\mathbf{F} = \begin{pmatrix} F_\xi \\ \\ F_\eta \end{pmatrix} = \begin{pmatrix} cos\Omega t & sin\Omega t \\ \\ -sin\Omega t & cos\Omega t \end{pmatrix} \begin{pmatrix} P_x \\ \\ P_y \end{pmatrix} = \mathbf{T}(\Omega t)\mathbf{P} \tag{23}$$

Thus :

$$\mathbf{P} = \mathbf{T^{-1}}(\Omega t)\mathbf{F} \tag{24}$$

Inserting these transformations of forces and deflections into equation (21), we obtain the stiffness matrix $\mathbb{K}(\mathbf{U})$ expressed in the inertial frame.

$$\mathbb{K}(\mathbf{U}) = \mathbf{T^{-1}}(\Omega t)\mathbf{K}(\mathbf{u})\mathbf{T}(\Omega t) \tag{25}$$

The construction process of the stiffness matrix $\mathbf{K}(\mathbf{u})$ of the cracked shaft element lead to a skew-symmetric matrix :

$$\mathbf{K}(\mathbf{u}) = -\mathbf{K}^t(\mathbf{u}) \tag{26}$$

which is invariable by rotation. We have :

$$\mathbb{K}(\mathbf{U}) = \mathbf{K}(\mathbf{u}) \tag{27}$$

Now we can write the dynamical equilibrium equations of the DeLaval rotor of Figure 6 as given by the Principal of Virtual Power :

$$\mathbf{M\ddot{u}} + \mathbf{D\dot{u}} + \mathbf{K}(\mathbf{u})\dot{\mathbf{u}} = \mathbf{P_0} + \mathbf{P_u} \tag{28}$$

or :

$$\begin{pmatrix} m & \\ & m \end{pmatrix} \begin{pmatrix} \ddot{\mathrm{U}} \\ \ddot{\mathrm{V}} \end{pmatrix} + \begin{pmatrix} D & \\ & D \end{pmatrix} \begin{pmatrix} \dot{\mathrm{U}} \\ \dot{\mathrm{V}} \end{pmatrix} + \frac{48\pi ER^3}{L^2} \begin{pmatrix} \frac{R}{L} - k_{\xi\xi}(\psi) & \frac{1}{2}k'_{\xi\xi}(\psi) \\ \\ -\frac{1}{2}k'_{\xi\xi}(\psi) & \frac{R}{L} - k_{\xi\xi}(\psi) \end{pmatrix} \begin{pmatrix} \mathbf{U} \\ \\ \mathbf{V} \end{pmatrix} = \begin{pmatrix} mg \\ \\ 0 \end{pmatrix} + \varepsilon m_u \Omega^2 \begin{pmatrix} cos(\beta + \Omega t) \\ \\ sin(\beta + \Omega t) \end{pmatrix} \tag{29}$$

$\mathbf{P_0}$ is the disc weight and $\mathbf{P_u}$ is the umbalance forces due to the umbalance mass m_u at ε from G (Figure 6).

$D = 2dmw_0$ is the viscous damping coefficient, d the reduced (dimensionless) damping coefficient and $w_0 = \sqrt{\frac{k_0}{m}}$ the natural frequency of the uncracked structure.

The shaft orbits presented in Figure 7 show that the superharmonic resonance phenomena presence when the rotating frequency passes through entire divisions of the critical speed w_0. When $\xi \approx \frac{\Omega}{n}$, the vibratory amplitude of n^{th} harmonic reaches higher levels, cf. Figure 7. At starting up, coasting down the

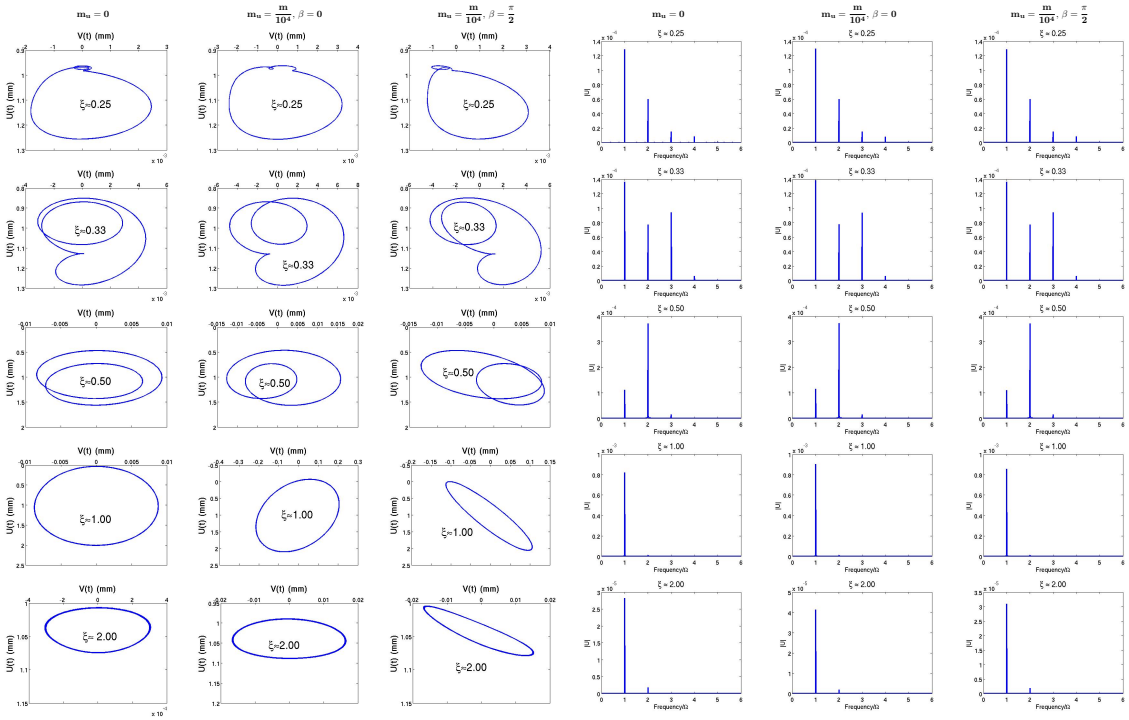

FIGURE 7 – Examples of the rotor orbits and amplitude spectra, $\xi = \frac{\Omega}{w_0}$, $\frac{a}{R} = 1$, $d = 0.03$

observation of this superharmonic resonances at subcritical rotor frequencies represents a good indication of crack presence.

In the normal operating conditions, the turbines are rotating at constant frequency, and here a crack growth could be depicted by monitoring the evolution of the static deflection and the levels of the first and second harmonics (today's vibration minus vibration a fortnight before), cf. Figure 8. These vibratory parameters are very reliable for early detecting the presence and propagation of cracks.

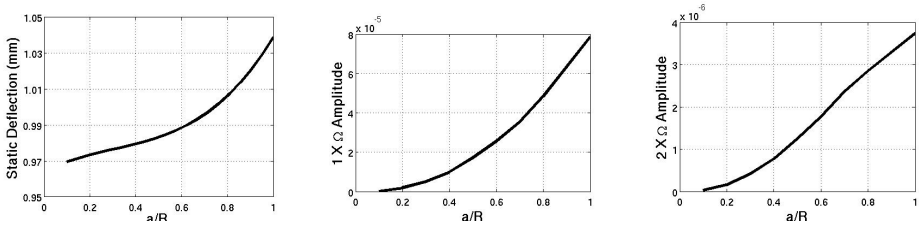

FIGURE 8 – Evolution of vibratory parameters with crack depth, $\xi = 1.50$, $d = 0.03$

4 Stability analysis

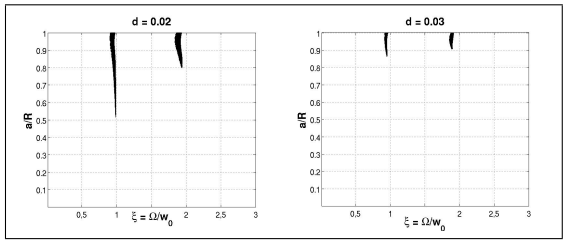

FIGURE 9 – Stable and unstable (hatched) zones evolution for $d = 0.02$ and $d = 0.03$

In this work, the stability of the cracked shaft of Figure 6 containing a straight tip crack at mid-span is analyzed using the Floquet method which is easy to implement numerically. Results for viscous dissipation $d \approx 2\ \%$ and $d \approx 3\ \%$, cf. Figure 9, show two principal instability areas : the first is located around the exact resonance ($\xi = 1$) and the second area (around $\xi = 2$) corresponds to subharmonic resonance.

It's important to note that even for weak viscous damping ($d \approx 2\ \%$) the stability of the cracked shaft is only slightly affected. When $d \approx 5\ \%$ the zones of instabilities disappear completely for cracks with depth going to half the transverse section ($\frac{a}{R} = 1$). A third zone of instability has been observed by many authors at the subcritical speed range ($\xi < 1.0$) when considering a switching crack model ([5]) or in the case of very deep breathing cracks and low dissipation ([6]). But for more realistic operating conditions like in this article, as noticed by [7, 2], this zone is free of chaotic, quasi-periodic or subharmonic response. Since for real machines the viscous damping is $\approx 3\%$, we can say that the effect of one propagating crack begins to threaten the stability only at important depth $\frac{a}{R} > 0.85$ and this on a narrow interval around $\Omega \approx w_0$ and $\Omega \approx 2 \times w_0$. The passage through these frequencies must be done with the greatest care especially when it comes to turn off the machines after a long period of uninterrupted service.

5 Conclusions

In this article we have presented a systematic approach in dealing with the problem of modelling cracked rotating shafts. The breathing mechanism identification is the crucial step in the process and has to be made with the greatest care. To make this approach generic, we have opted for the identification of a dimensionless flexibility so that it can be used in similar configuration.

Once the additional flexibility due to the crack identified, we have introduced it in a 2 dof dynamical system of a DeLaval rotor with a breathing crack at midspan. All the typical features related to cracked rotors have been observed. We have noticed the superharmonic resonnace phenomena when the machine is operated at an entier division of the first critical frequency. Also, we have found that the increase of the vibrational levels of the first and second superharmonics accompagned by the growth of static deflection are reliable indicators of a propagating crack. We hope that the clarity of the different steps of the methodology presented here and the simplicity of its numerical implementation will make it the standard approach in dealing with cracked rotating shafts.

The next step will be to consider the case of multiple cracks affecting the same rotor at different positions along its axis. In this case, it would be wise to construct a beam-like finite element based on the development presented in this article. The new finite element will have a crack at midspan and will be inserted at the appropriate locations between classical beam elements to model a cracked region of the rotor. And this is what we are in the process of developing at this time by following the approach described by [4].

Références

[1] S. Andrieux and C. Varé. A 3d cracked beam model with unilateral contact- application to rotors. *European Journal of Mechanics, A/Solids*, 21 :793–810, 2002.

[2] S. El Arem. *Vibrations non-lineaires des structures fissurées : application aux rotors de turbines (in french)*. PhD thesis, Ecole Nationale des Ponts et Chaussées, 2006.

[3] S. El Arem. Shearing effects on the breathing mechanism of a cracked beam section in biaxial flexure. *European Journal of Mechanics, A/Solids*, 28 :1079–1087, 2009.

[4] S. El Arem and H. Maitournam. A cracked beam finite element for rotating shaft dynamics and stability analysis. *Journal of Mechanics of Materials and Structures*, 3(5) :893–910, 2008.

[5] R. Gasch. Dynamical behavior of a simple rotor with a cross-sectional crack. In *Vibrations in rotating machinery*, pages 123–128, I. Mech. E. Conference, London, 1976.

[6] Saber El Arem and Quoc Son Nguyen. Nonlinear dynamics of a rotating shaft with a breathing crack. *Annals of Solid and Structural Mechanics*, 3(1) :1–14, 2012.

[7] T. H. Patel and A. K. Darpe. Influence of crack breathing model on nonlinear dynamics of a cracked rotor. *J. Sound and Vibration*, 311 :953–972, 2008.